ORIGINAL ARTICLE

Hydrolyzable and biocompatible aliphatic polycarbonates with ether-functionalized side chains attached via amide linkers

Kazuki Fukushima [1,2,3] · Shunta Hakozaki[2] · Rongjian Lang[1] · Yuta Haga[2] · So Nakai[1] · Atsushi Narumi [2] ·
Masaru Tanaka[4] · Takashi Kato[1,5]

Abstract

Investigating polymer degradation mechanisms enables the establishment of controlled degradation techniques for the development of sustainable and recyclable materials. Hydration can play a crucial role in controlling the hydrolysis of polymers. Here, ether-functionalized aliphatic polycarbonates (APCs) susceptible to nonenzymatic hydrolysis were developed for application as biocompatible biomaterials. Among these polymers, those grafted with 2-methoxyethyl and 3-methoxypropyl side chains via an amide group were highly wettable, strongly interacted with water, and experienced almost complete hydrolysis in phosphate-buffered saline over 30 days, which was attributed to the hydrogen bonding between water and the amide/methoxy groups. In an alkaline medium, all amide-linked APCs were completely hydrolyzed within 30 days, regardless of the side-chain structure. In contrast, the nonamide-linked APCs and a representative aliphatic polycarbonate, poly(trimethylene carbonate), were minimally degraded in the buffer and experienced <31% degradation under alkaline conditions. The APC with the 3-methoxypropyl side chain exhibited platelet adhesion properties comparable to those of ether-functionalized APCs previously reported as blood-compatible polymers. Thus, our results demonstrate the effects of an amide linker on the hydration and hydrolytic properties of APCs and can help establish new design concepts for degradable polymers.

Introduction

Numerous environmental problems associated with synthetic polymers, including greenhouse gas emissions and marine microplastics [1–4], can potentially be solved by shifting to recyclable and sustainable alternatives [5–7]. Consequently, considerable attention has been given to the replacement of nondegradable functional polymers with degradable polymers and the further development of the latter, as exemplified by the use of aliphatic polyesters (e.g., polylactides and poly(hydroxyalkanoate)s) for single-use and short-term applications [8–11]. In particular, functional degradable polymers with tunable degradability, i.e., controllable degradation rate and timing, have been actively explored.

Several degradable polymers with functional side chains have been developed for biomedical devices used in nano- and regenerative medicine [12–14]. In the last two decades, side-chain-functionalized aliphatic polycarbonates (APCs) have emerged as a widespread platform for realizing functional degradable biomaterials [15–18]. Inspired by the commercially available blood-compatible polymer poly(2-methoxyethyl acrylate) (PMEA) and its analogs [19–22], we developed ether-functionalized APCs for potential use as stent coatings, surface layers of resorbable artificial blood vessels, and other components of blood-compatible biomedical devices [23–26]. The ether side groups enhance

✉ Kazuki Fukushima
k_fukushima@chembio.t.u-tokyo.ac.jp

1 Department of Chemistry and Biotechnology, School of Engineering, The University of Tokyo, 7-3-1 Hongo, Bunkyo-ku, Tokyo 113-8656, Japan

2 Department of Polymer Science and Engineering, Graduate School of Organic Materials Science, Yamagata University, 4-3-16 Jonan, Yonezawa, Yamagata 992-8510, Japan

3 Japan Science and Technology Agency (JST), PRESTO, 4-1-8 Honcho, Kawaguchi, Saitama, Japan

4 Institute for Materials Chemistry and Engineering, Kyushu University, 744 Moto-oka, Nishi-ku, Fukuoka 819-0395, Japan

5 Research Initiative for Supra-Materials, Shinshu University, Wakasato, Nagano 380-8553, Japan
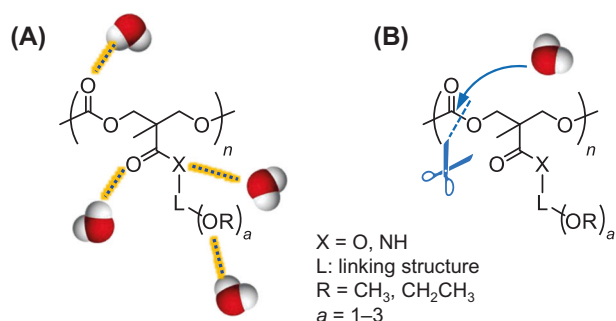
Fig. 1 Schematics of (**A**) hydration and (**B**) hydrolysis of the employed aliphatic polycarbonates (APCs)

hydration, helping to control the adsorption and denaturation of serum proteins and thus inhibiting platelet adhesion [27, 28]. This mechanism was also exemplified by a recently reported poly(*p*-dioxanone) derivative [29]. These studies yield important insights into the hydrolytic degradation of polymers, suggesting that hydration due to interactions with ether side groups facilitates the hydrolysis of polymer backbones composed of aliphatic ester and carbonate moieties [21, 29].

Poly(trimethylene carbonate) (PTMC) is a representative biodegradable APC widely used in commercialized biomaterials such as sutures [30] yet fairly stable for nonenzymatic hydrolysis [31]. Unlike its analogs that include oligo(ethylene glycol) moieties, PTMC is minimally degraded in alkaline solutions, suggesting that the degradability of the APC main chain is affected by the appended side chains [32]. The introduction of appropriate functional groups and structures renders APCs suitable for the fabrication of sustainable functional materials [33–35]. Accordingly, the hydrolyzability of such APCs in the absence of enzymes (or at low enzyme levels) is important for estimating the environmental impact of their disposal. Furthermore, the correlation of hydration properties with hydrolyzability may enable the control of the lifetime and stability of APC in aqueous environments and thus expand the application scope of these polymers.

Considering the above discussion, we investigated the relationship between the hydration and hydrolysis of APCs more deeply and enhanced these properties through structural optimization (Fig. 1) to help advance the controllable degradation of aliphatic polyesters and APCs. The extent of hydration induced by ether side groups varies depending on the carbon–oxygen ratio and the configuration of ether oxygen (e.g., distance from the main chain), as demonstrated by PMEA analogs [20, 22]. However, a similar systematic study has never been performed on APCs because of the difficulty in synthesizing analogs of equal quality and molecular weight. The investigated APCs were derived from 2,2-bis(hydroxymethyl)propionic acid (bis-MPA), as the resulting scaffolds can be efficiently grafted

with side-chain functionalities using the postpolymerization protocol developed by Engler et al. [36]. This approach enables the preparation of APCs with different types of ether side groups at the same chain length, thus avoiding tedious individual monomer synthesis. Six bis-MPA-based APCs with ether group–containing side chains linked to the main chain by an amide group (**P1**–**P6**) were synthesized to elucidate the effects of hydration on degradability and biological functions (Fig. 2). Moreover, we investigated the effects of the amide linker on hydration by comparison with those of a previously reported ether-functionalized APC bearing an ester linker (**P7**) [23], an APC with a methoxy side chain (**P8**) [25], and PTMC (**P9**).

Results and discussion

APC synthesis and characterization

The triflic or methanesulfonic acid–catalyzed ring-opening polymerization of **M1** yielded a precursor polymer (**P0**) with a sufficiently high number-average molecular weight ($M_n = 18.3 \times 10^3\,\mathrm{g\,mol^{-1}}$) and low molar-mass dispersity ($Đ_M = 1.14$), and subsequent side-chain (postpolymerization) amidation yielded **P1**–**P6** (Scheme 1) [36]. Figure 3 shows the ^{1}H nuclear magnetic resonance (NMR) spectrum of **P2** as a representative example. All amidation reactions were shown to be quantitative by ^{1}H NMR spectroscopy (Figs. S1–S6), although the reaction completion time depended on the side-chain structure, equaling 1 h for **P1**–**P3** and 3 h for **P4**–**P6**, possibly because of steric effects. This steric effect is associated with the nucleophilicity of the amine and the accessibility of the amine to unreacted sites in the polymer. The former is applicable to **P4** formation, where the amino group is sterically hindered by a tetrahydrofurfuryl group. A similar steric effect was found in our previous study to examine esterification between carboxylate anion and tetrahydrofurfuryl bromide [26]. The latter effect is explained by the formation of **P5** and **P6**, where the side groups attached to bulky gallate derivatives hinder the subsequent access of the amines to the neighboring pentafluorophenyl ester side groups of **P0**. These two mechanisms may induce the longer reaction times associated with the corresponding processes. The $Đ_M$ values of **P1**–**P6** were not significantly different from that of **P0**; i.e., amidation did not induce main-chain decomposition (Table 1 and Fig. S7).

P1–**P6** are amorphous substances with side-chain-dependent glass transition temperatures (T_g, 3–56 °C). The relatively high T_g values of **P4**–**P6** (>40 °C) were attributed to their bulky and rigid side chains (Table 1). The T_g of amide-linked **P1** was 40 °C greater than that of its ester-linked analog (**P7**), which was attributed to the amide group engaging in interchain hydrogen bonding.

**Fig. 2** Molecular structures of the employed APCs (**P1**–**P9**). PTMC = poly(trimethylene carbonate)
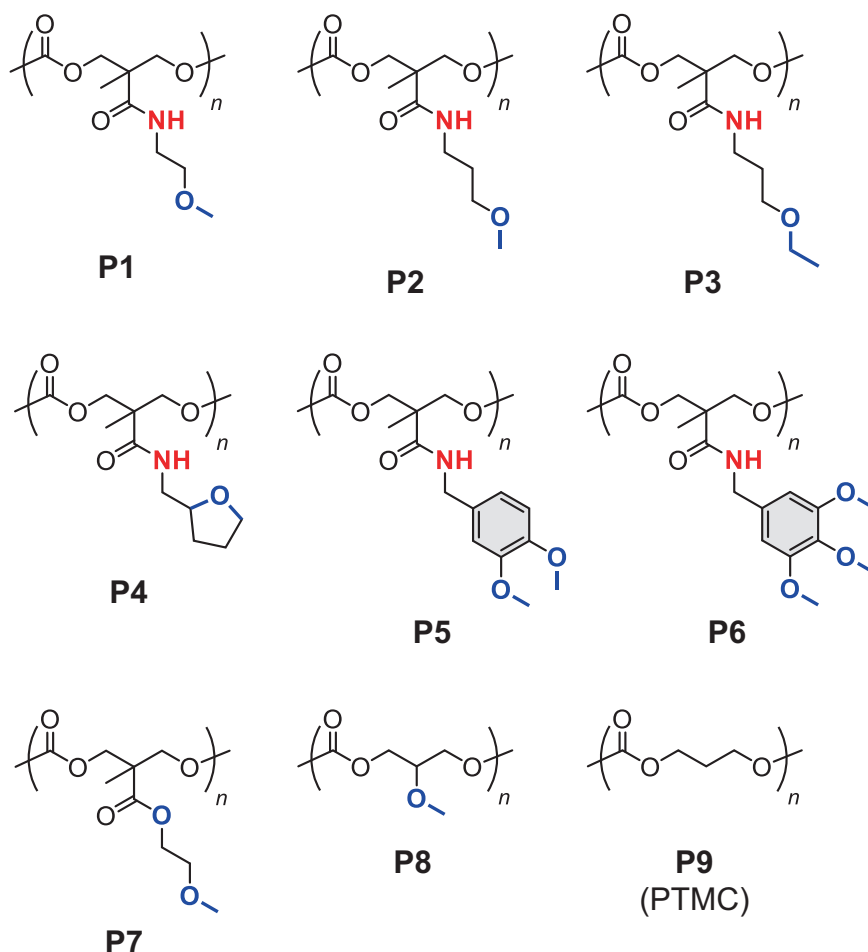
## Hydration properties of APCs

The hydration properties of the APCs were evaluated by differential scanning calorimetry (DSC) analysis and water contact angle measurements [27, 28]. Static water contact angles were measured for spin-coated samples using sessile-drop (θ_w) and captive-bubble (θ_{air}) methods. The θ_w of **P1** (53°) was 10° lower than that of **P7** (63°) (Table 1); i.e., the surface of the former polymer was more hydrophilic. For **P1**–**P6**, θ_w was closely correlated with the side-chain structure and increased with the number of carbon atoms and the carbon-to-oxygen ratio. The differences among the θ_{air} values of **P2**–**P6** were minor compared to those among the corresponding θ_w values. **P2**–**P6** had higher θ_{air} values (i.e., more hydrophilic surfaces in water) than did **P7**–**P9**. The above results reflect the effects of the amide linker on hydration. Considering that in the ideal scenario, $\theta_w = 180° - \theta_{air}$ [37], the difference between the measured θ_w and the value calculated as $180° - \theta_{air}$ ($= \theta_{w\text{-calc.}}$) represents deviation from the theoretical value for hydrophilicity of a given surface in air or water. In fact, the θ_{air} values of **P1** and **P2** are lower than expected, while the θ_w values of

P5 and **P6** are higher than expected. These results are likely related to the mobility of the amide-linked side-chain ether groups in contact with water. In particular, **P1** and **P2** may engage in distinctive interactions with water because of the configuration of their amide and methoxy groups, which restricts side-chain motion in water. Based on the difference between **P1** and **P7**, the hydrogen-bond donor function of the amide N–H significantly contributes to the enhanced hydration of **P1** and **P2**, as does the methoxy group (Fig. 4A, D). Although the amide C = O also interacts with water, this interaction is omitted from the discussion on the effects of the amide N–H. Furthermore, the methoxy oxygen serves as a hydrogen-bond acceptor, which may lock the water molecule bound to the amide N–H (Fig. 4B, E). These mechanisms motivate the proposed intramolecular hydrogen-bonding modes of the side chains of **P1** and **P2** (Fig. 4C, F), which may be associated with their glass transition and response upon contact with water. The side chain of **P1** should theoretically be more hydrophilic than that of **P2** based on the carbon-to-oxygen ratio. However, because the θ_w value of **P2** was lower than that of **P1** (Table 1), we suspect that the populations of the double

Scheme 1 Syntheses of precursor polymers (**P0**) and ether-functionalized APCs (**P1–P6**)

Precursor polymer

Postpolymerization amidation

E: Ether-functionalized substituent
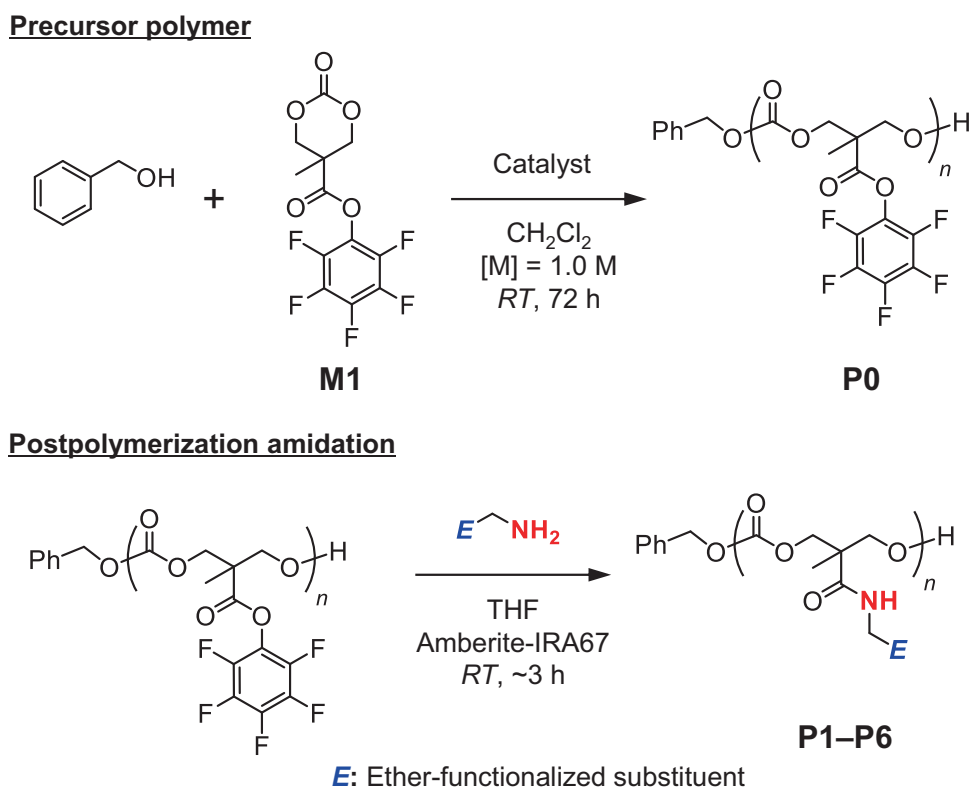
Fig. 3 ^{1}H nuclear magnetic resonance (NMR) spectrum (400 MHz) of **P2** in deuterated chloroform (CDCl$_3$; internal standard = tetramethylsilane (TMS))
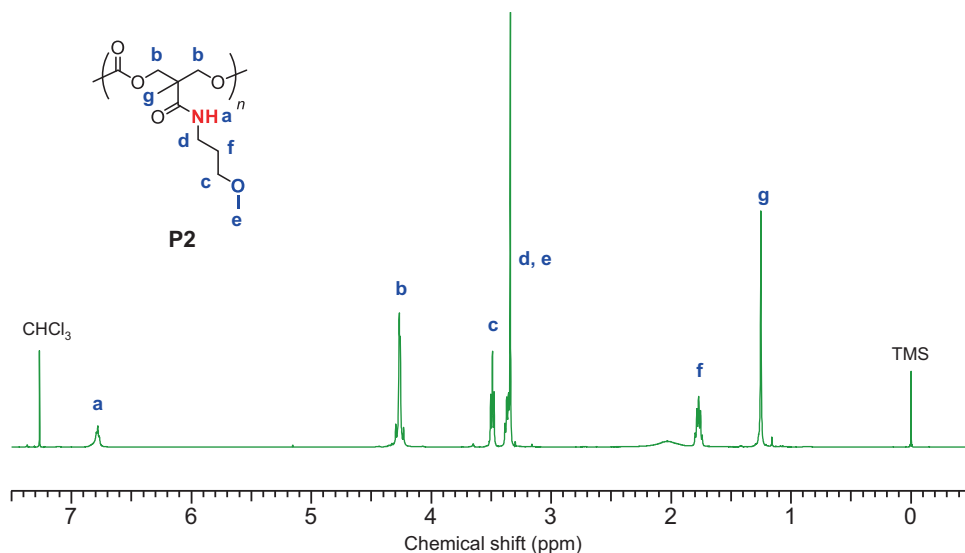
(Fig. 4B, E) and intramolecular (Fig. 4C, F) hydrogen-bonding modes for **P1** are greater than those for **P2**, which decreases the wettability and hydration.

DSC analysis of the hydrated polymers provided further insights into the polymer–water interactions. DSC peaks corresponding to the fusion and crystallization of water can appear at temperatures below 0 °C, depending on the above interactions, e.g., strong polymer–water interactions retard the crystallization of water, similar to cryoscopy. Figure 5

shows the DSC thermograms of hydrated APCs (**P1–P3, P7**) with near-equilibrium water contents. Hydrated **P4–P6** could be prepared from only the overhydrated state, and the corresponding DSC profiles are shown in Figure S8. The equilibrium water contents of **P1–P3** (~17 wt%) exceeded those of **P7** (5 wt%) [23] and previously developed ether-functionalized polymers [24–26], which demonstrated the beneficial effect of the amide linker on polymer hydration (Fig. 4). Furthermore, the heating DSC profiles of hydrated

P1–P4 exhibited exothermic peaks corresponding to cold crystallization of water at −40 to −10 °C (Figs. 5A–C and S8A), which is typically observed for hydrated PMEA and its derivatives [19, 22]. This cold crystallization is associated with biocompatibility, along with the crystallization of water at approximately −40 °C upon cooling observed for ether-functionalized APCs reported previously, including **P7** (Fig. 5D) [23–26]. Hydrated **P1–P4** are the first APCs revealed to exhibit cold crystallization of water by DSC analysis. The formation of water that underwent cold crystallization was mainly attributed to the

combination of amide and side-chain aliphatic ether groups (Fig. 4). Considering the cooling and heating of hydrated polymers, water crystallization during heating is more affected by interactions with the polymer structure (which mitigates freezing) than crystallization during cooling is. Thus, we concluded that the amide linker of **P1–P4** binds water more strongly than the ester linker of **P7**; therefore, the enhanced hydration yields cold crystallization of water. The extent of this hydration is reflected by the enthalpies of the cold crystallization of water, which are 17, 26, 13, and 6 J g^{-1} for hydrated **P1, P2, P3**, and **P4**, respectively (Figs. 5A–C and S8A). Given that the enthalpy of crystallization of water during cooling for hydrated **P7** is 4 J g^{-1} (Fig. 5D), the enhancement of the hydration properties of **P1** and **P2** by the amide linker is shown to be significantly high. Despite not explicitly appearing in the related thermograms, the glass transitions of hydrated **P1–P4** is expected to occur at temperatures below those of cold crystallization, which are considerably lower than those observed for dry states (Table 1). Accordingly, the amide linker in **P1–P4** was concluded to substantially improve the hydration properties.

Table 1 Characteristics of ether-functionalized APCs

	M_n[a] (kg mol^{-1})	$Đ_M$[a]	T_g (°C)[b]	Contact angle (°)[c] θ_w	θ_{air}	$\theta_{w\text{-calc.}}$[d]
P1	10	1.19	21	53 ± 3.9	116 ± 6.4	64
P2	11	1.22	8	32 ± 2.8	124 ± 6.7	56
P3	10	1.34	3	56 ± 2.2	122 ± 3.4	58
P4	10	1.22	28	49 ± 2.7	128 ± 5.7	52
P5	14	1.20	52	69 ± 1.8	125 ± 2.7	55
P6	14	1.20	56	63 ± 2.2	128 ± 2.7	52
P7	9	1.19	−19	63 ± 1.4	118 ± 1.2	62
P8	10	1.23	−9	73 ± 1.8	107 ± 2.7	73
P9	34	1.11	−17	76 ± 0.6	115 ± 1.5	65

[a]Measured by size-exclusion chromatography in tetrahydrofuran at 40 °C using polystyrene standards

[b]Extracted from second heating differential scanning calorimetry profiles

[c]Represented as the means ± standard deviations (n = three points × five specimens)

[d]Calculated as 180° − θ_{air}
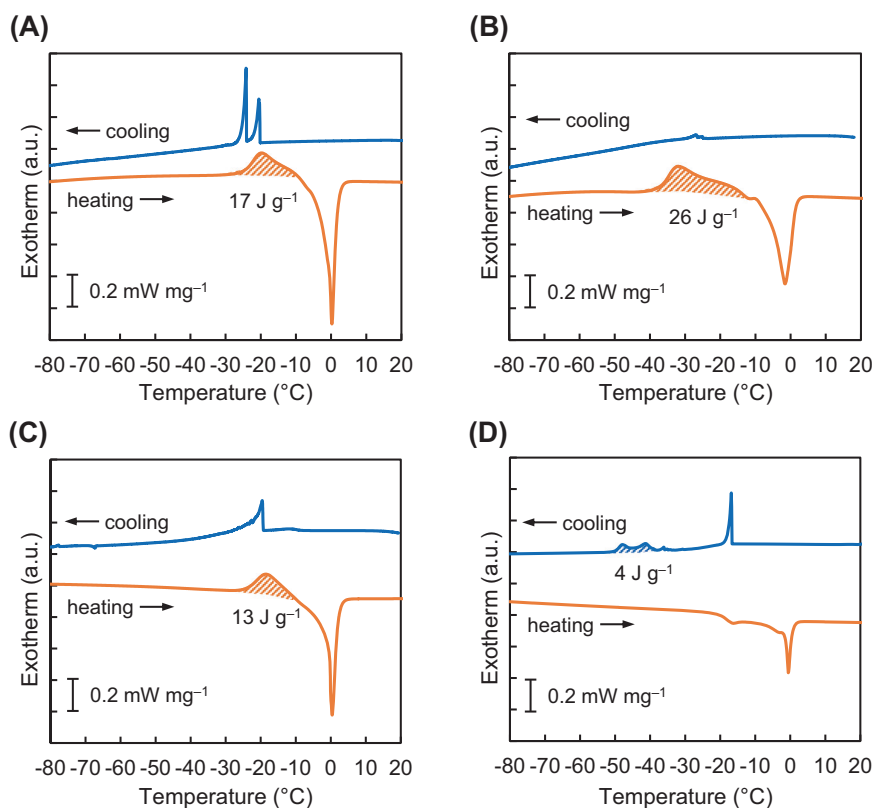
Hydrolytic degradation of APCs

Polymer degradation is often conducted at ≤25 °C and neutral pH, especially when marine and environmental degradability is simulated [38]. However, previously developed APCs exhibit low degradability under mild conditions [25]. Given that we aimed to understand the relationship between side-chain structure and hydrolytic properties rather than to verify marine and environmental degradability, APC hydrolyzability was evaluated under moderate heating (37 °C) in an


Fig. 4 Schematics of possible hydrogen-bonding modes of the side chains of **P1** (A–C) and **P2** (D–F). **A, D** Amide N–H and methoxy oxygen interact with water separately. **B, E** The amide N–H and methoxy oxygen lock a water molecule. **C, F** Intramolecular hydrogen bonding in the side chain
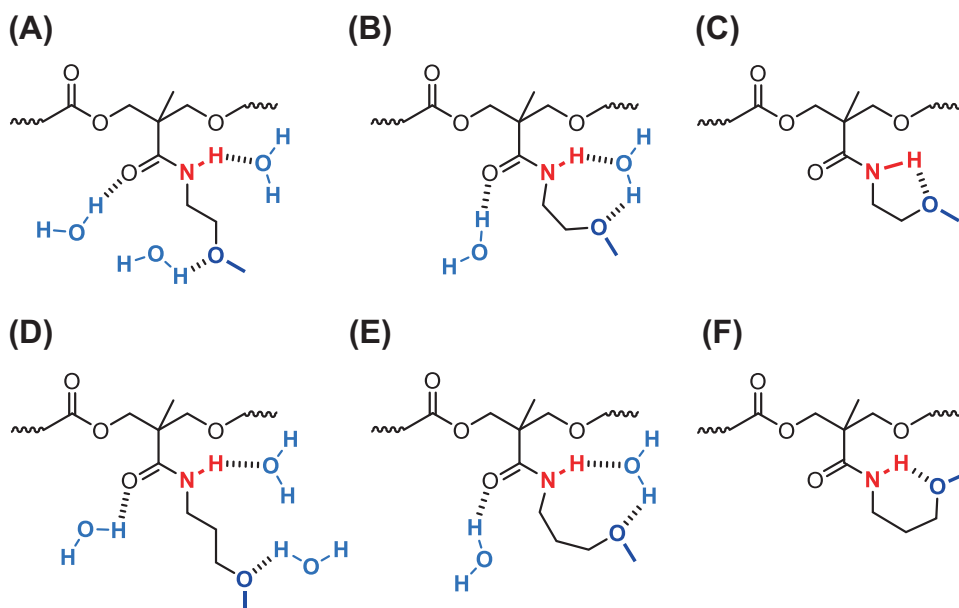
Fig. 5 Differential scanning calorimetry profiles of hydrated (**A**) **P1**, (**B**) **P2**, (**C**) **P3**, and (**D**) **P7**. The areas of exothermic peaks on the heating (**A**–**C**) and the cooling (**D**) are shaded. The water contents are 17 wt% for **P1**–**P3** and 5 wt% for **P7**

Fig. 6 Hydrolytic degradation of APCs in D_2O. **A** Schematic degradation of the amide-linked APCs **P***x*, affording degradates **D(P***x*) (*x* = 1–6). **B**–**D** Typical appearances of degradation solutions at 30 days. **B P1** was completely hydrolyzed in NaOD–D_2O. **C P7** was partially degraded in NaOD–D_2O with residues attached to the stir bar. **D P4** was partly degraded in phosphate-buffered saline–D_2O with insoluble unreacted particles
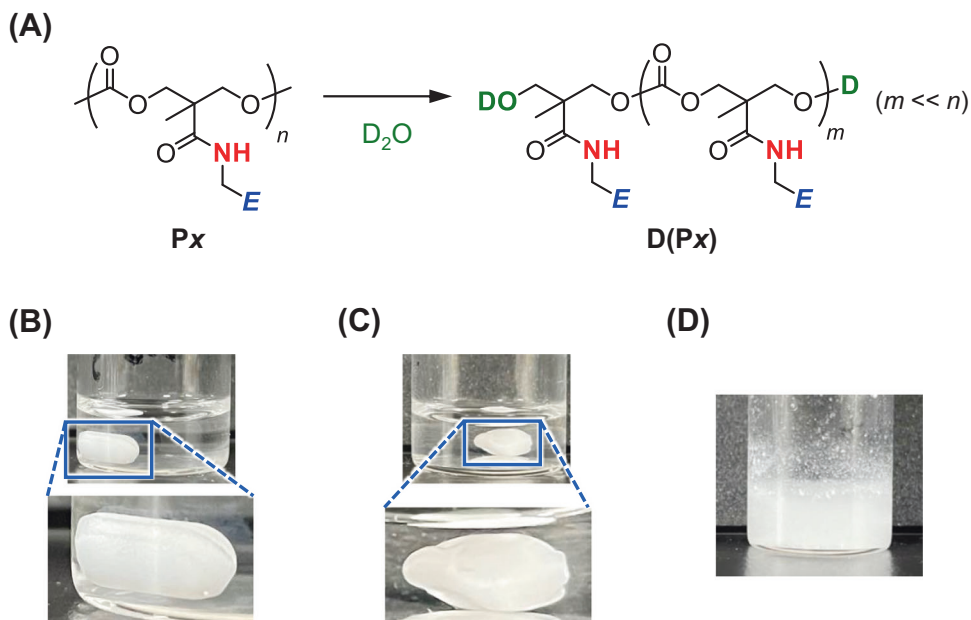
alkaline solution and in phosphate-buffered saline (PBS) formulated in deuterium oxide (D_2O) (Fig. 6A). The former environment corresponded to accelerated degradation conditions and was used for comparison with PTMC, which is stable under such conditions [32], while the latter environment better represented physiological conditions relevant to biomaterials applications. Because none of the tested polymers were water soluble, their degradation proceeded inhomogeneously. These degradation processes were examined by visual inspection (Figs. 6B–D and S9) and ^1H NMR spectroscopy using internal standards to estimate the amounts of soluble degradates (Figs. S10–S27).

Alkaline hydrolysis was conducted in 0.1 M NaOD in D_2O. The degradation behavior of amide-linked APCs

(**P1**–**P6**) was different from that of nonamide-linked APCs (**P7**–**P9**). The alkaline hydrolyses of **P1**–**P6** were complete (i.e., the solution became transparent) after 25 days (Fig. 6B and Table 2). The ^{1}H NMR spectra of the related degradates revealed that amide-linked bis-MPA derivatives were the major products ($m = 0$ for **D(Px)** in Figs. 6A, 7A and S10–S15), and the peaks of the minor products were tentatively assigned to short-chain oligomers. The size-exclusion chromatography (SEC) profiles of the degradates showed single peaks appearing considerably later (at 10–11 min) than those of the original polymers (Fig. S28A–F). Thus, no polymers were contained in the degradates of **P1**–**P6** produced in 0.1 M NaOD–D$_2$O. In contrast, the alkaline hydrolyses of **P7**–**P9** resulted in the formation of aggregates around stir bars (Figs. 6C and S9A). The water-soluble degradates in the corresponding supernatants were identified as monomer-derived diols, e.g., bis-MPA and 2-methoxyethanol, in the case of **P7**, which indicated that the ester linker was cleaved by alkaline hydrolysis (Figs. S16–S18). The degradation percentages of **P7**–**P9** were calculated to be 28%, 30%, and 2.5%, respectively, based on the integrated NMR signals and dimethyl sulfone (Me$_2$SO$_2$) as the internal standard (Table 2). The percentages of residual **P7**–**P9** calculated from the weights of the related dry residues were almost complementary (e.g., the values added to be 100%) to those of the soluble degradates (Table 2). These results are consistent with those of our previous studies, in which ether-functionalized APCs were degraded to a greater extent than PTMC was [25].

P1 and **P2** were susceptible to hydrolysis in PBS–D$_2$O, yielding transparent solutions with low residual polymer contents after 30 days (Table 2 and Fig. S9B). For **P3**–**P9**,

hydrolysis was considerably slower than that for **P1** and **P2**. After 30 days, the residues of **P3** and **P7**–**P9** were present as aggregates around stir bars (Figs. 6C and S9B), while those of **P4**–**P6** were dispersed in the solution as small particles (Figs. 6D and S9B). The supernatants (separated by centrifugation for **P4**–**P6**) were characterized by ^{1}H NMR spectroscopy, which revealed that the soluble degraded compounds resembled those formed under alkaline conditions (Figs. 7B and S19–S27). The degradation percentages of **P1**–**P6** depended on the side-chain structure (Table 2), i.e., exceeded 80% for **P1** and **P2** and were as low as ~20% for **P3** and **P4**. Like **P7**–**P9**, **P5** and **P6** were difficult to hydrolyze under neutral conditions. The residual polymer percentages showed the opposite trend, i.e., those of **P7**–**P9** were close to 100%, and those of **P3** and **P4** were 77% and 73%, respectively. The **P5** and **P6** residues were not fully recovered by centrifugation because of the very small particle size, and their contents (67% and 78%, respectively) were therefore underestimated. The SEC profiles of the **P3** and **P4** residues exhibited decreased molecular weights (Fig. S28C, D), which was indicative of bulk erosion–type degradation, whereas the molecular weights of the residual **P5**–**P8** were unchanged (Fig. S28E–H). This degradation trend was closely associated with polymer hydration properties, such as water contact angles (θ_w in Table 1); that is, more hydrated polymers were degraded faster. The rapid degradation of hydrophilic **P1** and **P2** was attributed to the formation of a surface-localized swollen phase where the polymer chains underwent bulk erosion-type random scission by water.

A bis-MPA-based APC with ester-linked ammonium side chains was previously reported to undergo complete hydrolysis in PBS–D$_2$O within 24 h because the ammonium side chains serve as nucleophiles and catalysts [39]. However, the high hydrolyzability of **P1** and **P2** could not be rationalized in the same way, as their hydrolysis was predominantly facilitated by polymer hydration enhanced by the amide linker and methoxy groups (Fig. 4). The hydrolysis of the examined APCs in PBS–D$_2$O may be divided into two groups according to their hydration properties: **P1**–**P4** and **P5**–**P9**. **P1**–**P4** were hydrolyzed to some extent (>16%) and exhibited cold crystallization of water in the hydrated state, whereas **P5**–**P9** showed no such crystallization and remained almost intact after hydrolysis (~2.7%). Preliminarily, we obtained a tendency for the degradation percentages to increase with increasing enthalpy during the crystallization of water (Fig. S29). However, further investigations should be performed to reach a quantitative conclusion by adopting spectroscopic analyses of the adsorption behavior of water to polymers [27]. Consequently, we clarified the impact of hydration (synergistically enhanced by amide and aliphatic ether groups) on APC hydrolysis.

Table 2 Percentages of soluble degradates and residual weights of APCs after hydrolysis at 30 days

	0.1 M NaOD		Phosphate-buffered saline	
	Degradates in supernatant (%)[a]	Residual weight (%)	Degradates in supernatant (%)[a]	Residual weight (%)
P1	>99 (10 d)	~0	93 (25 d)	~0
P2	>99 (18 d)	~0	82	~0
P3	>99 (18 d)	~0	16	77
P4	>99 (18 d)	~0	20	73
P5	>99 (18 d)	~0	1.6	67[b]
P6	>99 (25 d)	~0	2.2	78[b]
P7	28	69	2.7	95
P8	30	71	2.1	95
P9	2.5	96	0.5	>99

[a]Determined by ^{1}H NMR spectroscopy using Me$_2$SO$_2$ as the internal standard

[b]Residues were not fully recovered because of their small particle size

**Fig. 7** ^{1}H NMR spectra of hydrolysates of **P2** in (**A**) NaOD–D$_2$O and (**B**) PBS–D$_2$O (internal standards = dimethyl sulfone (Me$_2$SO$_2$) and sodium 3-(trimetylsilyl)-1-propane-1,1,2,2,3,3-d_6-sulfonate (DSS-d_6))
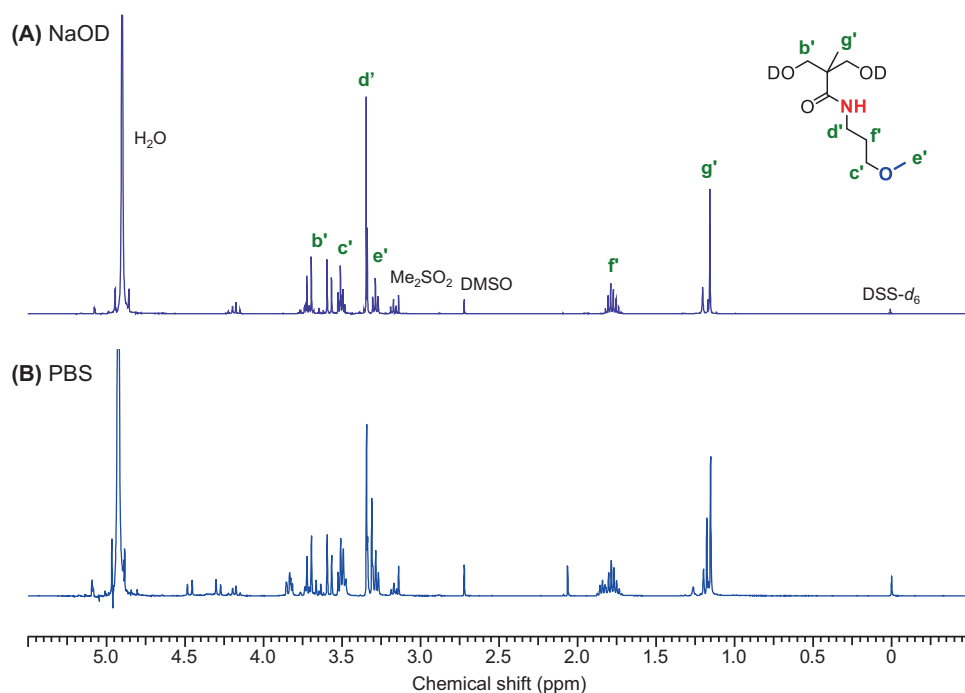
Platelet adhesion properties of APCs

The platelet adhesion properties of the APCs were evaluated for spin-coated substrates by a method previously used for other ether-functionalized polymers [19–26]. A platelet suspension was placed on the polymer surface, and the adherent platelets were observed by scanning electron microscopy (SEM; Fig. S30) and quantified (Fig. 8). The amide-linked APCs (excluding **P2**) demonstrated higher adherent platelet counts than did **P7** and PMEA, which were previously reported as blood-compatible polymers [19, 23]. For **P1**–**P7**, the number of adherent platelets increased with increasing number of side-chain carbons. **P2** showed minimally lower platelet adhesion than did **P1**, which is in line with a previous report on acrylate analogs with 2-methoxyethyl and 3-methoxypropyl groups [22]. These results indicated that the amide linker had no adverse effect on platelet adhesion despite the potential influence of hydrogen bonding between the amide linker and biomolecules such as serum proteins. **P3** and **P4** exhibited stronger platelet adhesion than did **P1, P2**, and **P7**, likely because of the greater hydrophobicity of the side chains in the former case. The alkyl aryl ether structures in **P5** and **P6**, which have never been assessed for platelet adhesion, did not efficiently lower platelet adhesion despite these molecules containing two and three methoxy groups, respectively. These results were also attributed to the hydration properties of the APCs (Table 1 and Figs. 5 and S8).

The desired degradation time of biomaterials in vivo depends on the device. Degradation of **P1** and **P2** is
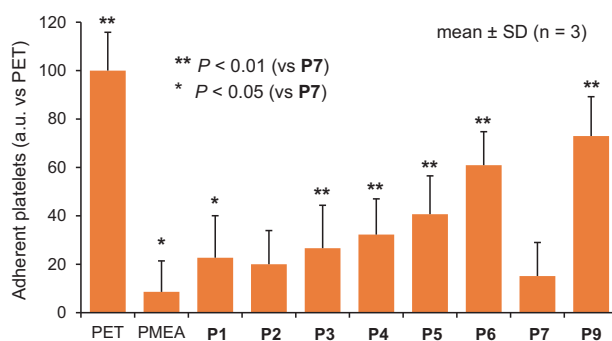
Fig. 8 Number of adherent platelets on polymer substrates spin-coated on poly(ethylene terephthalate) sheets

completed in a month, which may be shorter than the duration (over one month) needed for blood-contacting devices such as stent coatings and blood vessels [40]. In contrast, **P7** is less susceptible to enzymatic hydrolysis than **P9** is [23], which usually stays in the body for several months to a few years, depending on its molecular weight [30]. The present study yields **P2**, which exhibited high blood compatibility comparable to **P7**, as well as faster hydrolyzability. The combination of **P2** and **P7**, including copolymerization, ultimately enables the production of highly blood-compatible polymers with fine-tuned degradation properties.

Conclusion

Six APCs with ether-functionalized side chains grafted via an amide linker were prepared by postpolymerization

functionalization, which enabled the efficient grafting of ether-functionalized side chains without side reactions and main-chain cleavage. The amide linker provided several advantages stemming from hydrogen bonding. For example, compared to nonamide-linked analogs, amide-linked APCs showed higher T_g values and better hydration and hydrolytic properties. The introduction of the amide linker increased hydrolyzability by enhancing molecular interactions with water and promoting the hydrolysis of carbonate bonds. Thus, our results demonstrate the potential of side-chain engineering for preparing hydrolyzable APCs and pave the way for the purposeful design of polymers with tunable degradability.

Experimental section

Materials

All reagents used were purchased from Tokyo Chemical Industry (Tokyo, Japan), Sigma–Aldrich Japan (Tokyo, Japan), Fujifilm Wako Pure Chemical (Tokyo, Japan), Kanto Chemical (Tokyo, Japan), and Nacalai Tesque (Kyoto, Japan) and were used as received unless otherwise stated. Dehydrated tetrahydrofuran (THF) and dichloromethane (CH_2Cl_2) were supplied by a solvent supply system (Kanto Chemical, water content <10 ppm). PBS (pH 7.4) was prepared by dissolving tablets of phosphate buffer salts (Takara Bio, Tokyo, Japan) in ultrapure water. A glutaraldehyde solution (1%) was prepared by diluting 25% aqueous glutaraldehyde (Wako Pure Chemical) with PBS.

The reference polymers, namely, **P7** ($M_n = 9 \, kg \, mol^{-1}$, $Đ = 1.19$), **P8** ($M_n = 10 \, kg \, mol^{-1}$, $Đ = 1.23$), **P9** ($M_n = 34 \, kg \, mol^{-1}$, $Đ = 1.11$), and PMEA ($M_n = 21 \, kg \, mol^{-1}$, $Đ = 2.66$), were prepared as described elsewhere [19, 23, 25].

Measurements

^{1}H, ^{13}C, and ^{19}F NMR spectra were acquired on a JEOL JNM-ECX400 spectrometer at 400, 100, and 376 MHz, respectively. Deuterated chloroform ($CDCl_3$) and D_2O were used as solvents, and tetramethylsilane and sodium 3-(trimethylsilyl)-1-propane-1,1,2,2,3,3-d_6-sulfonate were used as internal standards. M_n and $Đ_M$ were estimated by SEC measurements, which were performed at 40 °C using THF (eluent) and an integrated SEC unit (Malvern Viscotek TDAmax) equipped with three TSK-gel (one G2000HHR and two GMHHR-H) columns connected in series and a refractive-index detector. M_n and $Đ_M$ were calibrated using polystyrene standards (580 to $2.2 \times 10^6 \, g \, mol^{-1}$). SEC measurements were also performed at 40 °C in N,N-dimethylformamide (DMF) containing 10 mM LiBr using an integrated SEC unit

(HLC-8420 EcoSEC Elite, Tosoh, Tokyo, Japan) with two TSK-gel columns (SuperAWM-H) connected in series and equipped with refractive index and ultraviolet (UV) detectors (UV-8420). In this case, poly(ethylene oxide) standards with $M_n = 2.4 \times 10^4 – 7.9 \times 10^5$ were used for calibration. DSC measurements (Hitachi High-Tech Science X-DSC7000) were performed at heating and cooling rates of 5 °C min^{-1} under nitrogen for specimens weighing 3–5 mg. Hydrated samples were prepared by immersion in ultrapure water at 20–25 °C for at least 24 h before the measurement. No weight loss occurred during the measurement.

Synthesis of P1

The precursor polymer (**P0**) was prepared as described elsewhere [36]. **P0** (300 mg, 0.92 mmol) was dissolved in THF (1.5 mL) containing Amberlite-IRA67 (161 mg). The dispersion was slowly supplemented with a solution of 2-methoxyethylamine (72.7 mg, 0.97 mmol) in THF (1.0 mL) at 0–5 °C and stirred at 20–25 °C. After the conversion exceeded 90% (^{1}H NMR control), the solution was filtered to remove the resin, and the filtrate was evaporated. The residue was dissolved in CH_2Cl_2 (2 mL) and reprecipitated by the addition of hexane (15 mL). Pentafluorophenol-containing precipitates were redissolved in CH_2Cl_2 (10 mL), and the solutions were washed with a saturated aqueous solution of $NaHCO_3$ (10 mL) or passed through Amberlite-IRA67. The organic phase was then concentrated under vacuum to yield **P1** as a white solid (124 mg, 62%). ^{1}H NMR (400 MHz, $CDCl_3$): δ 6.56–6.40 (br, N$\underline{H}$), 4.29 (s, C$\underline{H_2}$O), 3.45 (s, NHC$\underline{H_2}$C$\underline{H_2}$OCH$_3$), 3.35 (s, OC$\underline{H_3}$), 1.28 (s, C$\underline{H_3}$). ^{13}C NMR (100 MHz, $CDCl_3$): δ 171.7, 154.3, 70.9, 69.9, 58.8, 46.3, 39.5, 17.4.

Synthesis of P2

The reaction was performed as described for **P1** using 3-methoxypropylamine (84.6 mg, 0.95 mmol) instead of 2-methoxyethylamine. The product was obtained as a transparent liquid (107 mg, 50%). ^{1}H NMR (400 MHz, $CDCl_3$): δ 6.88–6.72 (m, N$\underline{H}$), 4.38–4.16 (m, C$\underline{H_2}$O), 3.49 (t, $J = 5.66$ Hz, C$\underline{H_2}$OCH$_3$), 3.41–3.31 (m, NHC$\underline{H_2}$, CH$_2$OC$\underline{H_3}$), 1.77 (quin, $J = 5.89$ Hz, C$\underline{H_2}$), 1.25 (s, C$\underline{H_3}$). ^{13}C NMR (100 MHz, $CDCl_3$): δ 171.4, 154.4, 71.8, 69.9, 58.7, 46.2, 38.6, 28.5, 17.2.

Synthesis of P3

The reaction was performed as described for **P1** using 3-ethoxypropylamine (99.1 mg, 0.96 mmol) instead of 2-methoxyethylamine. The product was obtained as a transparent viscous solid (147 mg, 65%). ^{1}H NMR (400 MHz,

CDCl$_3$): δ 6.80 (t, $J = 4.98$ Hz, N$\underline{H}$), 4.32–4.19 (m, C$\underline{H_2}$O), 3.58–3.43 (m, C$\underline{H_2}$OC$\underline{H_2}$CH$_3$), 3.38 (q, $J = 5.59$ Hz, NHC$\underline{H_2}$), 1.87–1.71 (m, CH$_2$C$\underline{H_2}$CH$_2$), 1.26 (s, C$\underline{H_3}$), 1.21 (t, $J = 7.02$ Hz, CH$_2$C$\underline{H_3}$). ^{13}C NMR (100 MHz, CDCl$_3$): δ 171.3, 154.4, 70.0, 66.6, 46.3, 39.0, 28.8, 17.2, 15.3.

Synthesis of P4

The reaction was performed as described for **P1** using tetra-hydrofurfurylamine (95.6 mg, 0.95 mmol) instead of 2-methoxyethylamine. The product was obtained as a white solid by precipitation from hexane/Et$_2$O (1:1, v/v) (126 mg, 56%). ^{1}H NMR (400 MHz, CDCl$_3$): δ 6.63–6.41 (br, N$\underline{H}$), 4.34–4.22 (m, C$\underline{H_2}$O), 4.02–3.91 (m, C$\underline{H}$), 3.89–3.68 (m, OC$\underline{H_2}$CH$_2$), 3.63–3.47 (m, NHC$\underline{H_a}$H$_b$), 3.28–3.09 (m, NHCH$_a\underline{H_b}$), 2.05–1.82 (m, C$\underline{H_2}$CH$_2$, CH$_2$C$\underline{H_a}$H$_b$), 1.60‑1.45 (m, CH$_2$CH$_a\underline{H_b}$), 1.28 (s, C$\underline{H_3}$). ^{13}C NMR (100 MHz, CDCl$_3$): δ 171.7, 154.3, 77.6, 69.9, 68.2, 46.4, 43.4, 28.6, 25.9, 17.4.

Synthesis of P5

The reaction was performed as described for **P1** using 3,4-dimethoxybenzylamine (161 mg, 0.96 mmol) instead of 2-methoxyethylamine. The product was obtained as a white solid (224 mg, 79%). ^{1}H NMR (400 MHz, CDCl$_3$): δ 6.80–6.70 (m, Ar–$\underline{H}$), 6.61–6.50 (br, N$\underline{H}$), 4.32 (d, $J = 4.98$ Hz, NHC$\underline{H_2}$), 4.25 (s, C$\underline{H_2}$O), 3.79 (s, OC$\underline{H_3}$), 1.22 (s, C$\underline{H_3}$). ^{13}C NMR (100 MHz, CDCl$_3$): δ 171.5, 154.3, 149.1, 148.4, 130.7, 119.8, 111.4, 111.2, 69.7, 55.9, 46.4, 43.4, 17.5.

Synthesis of P6

The reaction was performed as described for **P1** using 3,4,5-trimethoxybenzylamine (192 mg, 0.98 mmol) instead of 2-methoxyethylamine. The product was obtained as a white solid (214 mg, 69%). ^{1}H NMR (400 MHz, CDCl$_3$): δ 6.79–6.61 (br, N$\underline{H}$), 6.44 (s, Ar–$\underline{H}$), 4.41–4.17 (m, NHC$\underline{H_2}$, C$\underline{H_2}$O), 3.82–3.72 (m, OC$\underline{H_3}$), 1.23 (s, C$\underline{H_3}$). ^{13}C NMR (100 MHz, CDCl$_3$): δ 171.7, 154.4, 153.3, 137.0, 134.1, 104.5, 69.7, 60.8, 56.1, 46.4, 43.7, 17.4.

Measurement of static contact angles

Contact angles were measured by sessile-drop and captive-bubble methods using a contact angle meter (Drop Master DM-501, Kyowa Interface Science, Japan) and polymer-coated substrates prepared as reported previously [23, 25, 26]. The contact angles were read 30 s after the deposition of a water droplet (2 μL) or air bubble (2 μL). Ultrapure water was used for both measurements, which were performed at three different points per substrate using five substrates per polymer.

Hydrolytic degradation test

Hydrolytic degradation was monitored by ^{1}H NMR spectroscopy using PBS–D$_2$O and NaOD–D$_2$O (Sigma–Aldrich, Tokyo, Japan). The polymer of choice (10 mg) was dissolved in chloroform in a 5-mL scintillation vial, and the solution was evaporated and dried under vacuum to form a filmy sample. The vial was charged with 1 mL of PBS–D$_2$O or 0.1 M NaOD–D$_2$O, and the mixture was stirred at 37 °C. The water-soluble degradates in the supernatants were detected via ^{1}H NMR at predetermined times and quantified using dimethyl sulfoxide and dimethyl sulfone (Sigma–Aldrich, Tokyo, Japan) as internal standards. The completion of degradation was confirmed by visual inspection. At the completion of degradation or after 30 days, the reactions were quenched by the addition of deuterated trifluoroacetic acid. The solutions containing no residues were directly characterized by NMR spectroscopy, whereas those containing residues were separated into supernatants and residues. The supernatants were characterized by ^{1}H NMR spectroscopy, and the residues were analyzed by SEC using 0.1 mM LiBr in DMF as the eluent. The tests were conducted twice for each sample to ensure reproducibility.

Platelet adhesion test

Platelet adhesion was quantified using the number of adherent platelets on APC-coated substrates according to a previously established procedure [23–26]. Briefly, a platelet suspension with a concentration of 4.0×10^7 cells cm^{-2} was placed on the polymer substrate, incubated for 1 h at 37 °C, and removed. The substrate was washed, and the adherent platelets were fixed with PBS containing 1% glutaraldehyde for SEM imaging (VE-9800, KEYENCE, Tokyo, Japan) at an acceleration voltage of 5 keV and magnification of 1500×. Observations were made for five randomly selected points per substrate, and three substrates were evaluated for each polymer. The number of adherent platelets was determined as the average of those manually counted in the SEM images (five points × three substrates).

Compliance with ethical standards

Conflict of interest The authors declare no competing interests.

References

1. https://www.oecd.org/environment/plastics/increased-plastic-leakage-and-greenhouse-gas-emissions.htm. Accessed 29 Sep. (2023).

2. Nicholson SR, Rorrer NA, Carpenter AC, Beckham GT. Manufacturing energy and greenhouse gas emissions associated with plastics consumption. Joule. 2021;5:673–86.

3. Jambeck JR, Geyer R, Wilcox C, Siegler TR, Perryman M, Andrady A, et al. Plastic waste inputs from land into the ocean. Science. 2015;347:768–71.

4. Watt E, Picard M, Maldonado B, Abdelwahab MA, Mielewski DF, Drzal LT, et al. Ocean plastics: environmental implications and potential routes for mitigation – a perspective. RSC Adv. 2021;11:21447–62.

5. Coates GW, Getzler YDYL. Chemical recycling to monomer for an ideal, circular polymer economy. Nat Rev Mater. 2020;5:501–16.

6. Iwata T, Gan H, Togo A, Fukata Y. Recent developments in microbial polyester fiber and polysaccharide ester derivative research. Polym J. 2021;53:221–38.

7. Kawada J, Kitou M, Mouri M, Ario T, Kato K. Invention of biobased polymer alloys and their application in plastic automobile parts. Polym J. 2023;55:753–60.

8. Fukushima K, Kimura Y. Stereocomplexed polylactides (Neo-PLA) as high-performance bio-based polymers: their formation, properties, and application. Polym Int. 2006;55:626–42.

9. Hsieh Y-T, Nozaki S, Kido M, Kamitani K, Kojio K, Takahara A. Crystal polymorphism of polylactide and its composites by X-ray diffraction study. Polym J. 2020;52:755–63.

10. Taguchi S, Matsumoto K. Evolution of polyhydroxyalkanoate synthesizing systems toward a sustainable plastic industry. Polym J. 2021;53:67–79.

11. Yamazaki S, Harada M, Watanabe Y, Lang R, Kato T, Haba O, et al. Crystallization of star-shaped poly(l-lactide)s with arm chains aligned in the same direction in two-dimensional crystals in a Langmuir monolayer. Langmuir. 2023;39:5486–94.

12. Gabirondo E, Sangroniz A, Etxeberria A, Torres-Giner S, Sardon H. Poly(hydroxy acids) derived from the self-condensation of hydroxy acids: from polymerization to end-of-life options. Polym Chem. 2020;11:4861–74.

13. Komatsu S, Sato T, Kikuchi A. Facile preparation of 2-methylene-1,3-dioxepane-based thermoresponsive polymers and hydrogels. Polym J. 2021;53:731–9.

14. Iwasaki Y, Yokota A, Otaka A, Inoue N, Yamaguchi A, Yoshitomi T, et al. Bone-targeting poly(ethylene sodium phosphate). Biomater Sci. 2018;6:91–5.

15. Fukushima K. Poly(trimethylene carbonate)-based polymers engineered for biodegradable functional biomaterials. Biomater Sci. 2016;4:9–24.

16. Fukushima K. Biodegradable functional biomaterials exploiting substituted trimethylene carbonates and organocatalytic transesterification. Polym J. 2016;48:1103–14.

17. Ajiro H, Haramiishi Y, Chanthaset N, Akashi M. Polymer design using trimethylene carbonate with ethylene glycol units for biomedical applications. Polym J. 2016;48:751–60.

18. Yu W, Maynard E, Chiaradia V, Arno MC, Dove AP. Aliphatic polycarbonates from cyclic carbonate monomers and their application as biomaterials. Chem Rev. 2021;121:10865–907.

19. Tanaka M, Motomura T, Kawada M, Anzai T, Kasori Y, Shiroya T, et al. Blood compatible aspects of poly(2-methoxyethylacrylate) (PMEA)–relationship between protein adsorption and platelet adhesion on PMEA surface. Biomaterials. 2000;21:1471–81.

20. Mochizuki A, Hatakeyama T, Tomono Y, Tanaka M. Water structure and blood compatibility of poly(tetrahydrofurfuryl acrylate). J Biomater Sci. 2009;20:591–603.

21. Nishida K, Anada T, Kobayashi S, Ueda T, Tanaka M. Effect of bound water content on cell adhesion strength to water-insoluble polymers. Acta Biomater. 2021;134:313–24.

22. Kobayashi S, Wakui M, Iwata Y, Tanaka M. Poly(ω-methoxyalkyl acrylate)s: Nonthrombogenic polymer family with tunable protein adsorption. Biomacromolecules. 2017;18:4214–23.

23. Fukushima K, Inoue Y, Haga Y, Ota T, Honda K, Sato C, et al. Monoether-tagged biodegradable polycarbonate preventing platelet adhesion and demonstrating vascular cell adhesion: A promising material for resorbable vascular grafts and stents. Biomacromolecules. 2017;18:3834–43.

24. Fukushima K, Honda K, Inoue Y, Tanaka M. Synthesis of antithrombotic poly (carbonate-urethane) s through a sequential process of ring-opening polymerization and polyaddition facilitated by organocatalysts. Eur Polym J. 2017;95:728–36.

25. Montagna V, Takahashi J, Tsai MY, Ota T, Zivic N, Kawaguchi S, et al. Methoxy-functionalized glycerol-based aliphatic polycarbonate: Organocatalytic synthesis, blood compatibility, and hydrolytic property. ACS Biomater Sci Eng. 2021;7:472–81.

26. Watanabe Y, Takaoka S, Haga Y, Kishi K, Hakozaki S, Narumi A, et al. Organic carboxylate salt-enabled alternative synthetic routes for bio-functional cyclic carbonates and aliphatic polycarbonates. Polym Chem. 2022;13:5193–9.

27. Tanaka M, Hayashi T, Shigeaki M. The roles of water molecules at the biointerface of medical polymers. Polym J. 2013;45:701–10.

28. Tanaka M, Kobayashi S, Murakami D, Aratsu F, Kashiwazaki A, Hoshiba T, et al. Design of polymeric biomaterials: The "intermediate water concept". Bull Chem Soc Jpn. 2019;92:2043–57.

29. Fukushima K, Ota Y, Kato T. Polydioxanone derivative bearing methoxy groups toward bio-functional degradable polymers exhibiting hydration-driven biocompatibility. Macromol Chem Phys. 2022;223:2200192.

30. Zhang Z, Kuijer R, Bulstra SK, Grijpma DirkW, Feijen J. The in vivo and in vitro degradation behavior of poly(trimethylene carbonate). Biomaterials. 2006;27:1741–8.

31. Brannigan RP, Dove AP. Synthesis, properties and biomedical applications of hydrolytically degradable materials based on aliphatic polyesters and polycarbonates. Biomater Sci. 2017;5:9–21.

32. Haramiishi Y, Chanthaset N, Kan K, Akashi M, Ajiro H. Contrast effect on hydrolysis of poly(trimethylene carbonate) depending on accelerated species due to the hydrophilic oligo(ethylene glycol) units at side groups. Polym Degrad Stab. 2016;130:78–82.

33. Watanabe Y, Kato R, Fukushima K, Kato K. Degradable and nanosegregated elastomers with multiblock sequences of biobased aromatic mesogens and biofunctional aliphatic oligocarbonates. Macromolecules. 2022;55:10285–93.

34. Saito K, Jehanno C, Meabe L, Olmedo-Martinez JL, Mecerreyes D, Fukushima K, et al. From plastic waste to polymer electrolytes

for batteries through chemical upcycling of polycarbonate. J Mater Chem A. 2020;8:13921–6.

35. Arai R, Seto K, Bell A, Sugimoto H. Synthesis of CO_2-derived polycarbonates with high glass transition temperatures. Polym J. 2018;50:301–7.

36. Engler AC, Ke X, Gao S, Chan JMW, Coady DJ, Ono RJ, et al. Hydrophilic polycarbonates: promising degradable alternatives to poly(ethylene glycol)-based stealth materials. Macromolecules. 2015;48:1673–78.

37. Prydatko AV, Belyaeva LA, Jiang L, Lima LMC, Schneider GF. Contact angle measurement of free-standing square-millimeter single-layer graphene. Nat Commun. 2018;9:4185.

38. Suzuki M, Tachibana Y, Kasuya K. Biodegradability of poly(3-hydroxyalkanoate) and poly(ε-caprolactone) via biological carbon cycles in marine environments. Polym J. 2021;53:47–66.

39. Fukushima K, Kishi K, Saito K, Takakuwa K, Hakozaki S, Yano S. Modulating bioactivities of primary ammonium-tagged anti-microbial aliphatic polycarbonates by varying length, sequence and hydrophobic side chain structure. Biomater Sci. 2019;7:2288–96.

40. Yamanaka H, Mahara A, Morimoto N, Yamaoka T. REDV-modified decellularized microvascular grafts for arterial and venous reconstruction. J Biomed Mater Res Part A. 2022;110:547–58.